ROYAL SOCIETY
OF CHEMISTRY

PAPER

Check for updates

A Zn₂-supported B₇ wheel structure for the global minimum of the B₇Zn₂ cluster†

Peter L. Rodríguez-Kessler [iD] *[a] and Alvaro Muñoz-Castro*[b]

In this work, we employ density functional theory (DFT) to explore the structure of boron clusters doped with two zinc atoms (B_7Zn_2 or Zn_2B_7). The results show that the most stable structure is a Zn_2 motif standing over a B_7 wheel, which is 0.89 eV lower in energy compared to the classical inverse-sandwich structure for B_7TM_2 (TM = transition metal) clusters. The characteristics of these systems are evaluated by the IR spectra to guide plausible experimental realization. In addition, density of states, and bonding characteristics were evaluated. Our results denote the formation of an intermediate Zn–Zn bond order given by the key electron-acceptor nature of the B_7 motif, leading to a depopulation of antibonding Zn–Zn orbitals and population of the respective bonding orbitals. Thus, the evaluation and use of more electron-deficient supporting ligands may trigger a quest for the design of plausible structures featuring larger Zn–Zn elusive bond orders in stable species.

1. Introduction

In the last decade, extensive theoretical and experimental research has been devoted to boron clusters. These clusters possess distinctive structural and electronic properties, as well as unique chemical bonding, which have attracted significant attention from the scientific community.[1,2] Due to their electron-deficient nature, boron clusters are a focal point in materials science and nanotechnology. This electron deficiency enables them to form a wide range of stable and metastable structures, making them highly versatile building blocks for various applications. Introducing dopants into these clusters with other elements can greatly alter their electronic, magnetic, and chemical properties, opening up possibilities for a wide range of applications.[3] While significant advances have been achieved in the experimental and theoretical investigation of transition-metal-doped boron clusters in recent years, studies on boron clusters doped with two transition metals are still in their early stages.[4] In 2006, Zhai *et al.* studied the electronic structure and chemical bonding of a binary $Au_2B_7^-$ cluster and found that the ground-state structure of $B_7Au_2^-$ ($B_7H_2^-$) can be viewed as adding two Au (H) atoms to the terminal B atoms of a higher-lying planar isomer of B_7^-. In 2014, Li and coworkers

reported a joint experimental and theoretical study on the $Ta_2B_6^{-/0}$ clusters and found that the most stable structures of both the neutral and anion are D_{6h} bipyramidal structures.[5] Wang and colleagues studied lanthanide-doped boron clusters, Ln_2B_n ($n = 7, 9$) and discovered inverse sandwich motifs within this series of chemical elements.[6] In particular, studies on M_2-doped boron clusters M_2B_7 involving alkaline earth metals (M = Be, Mg, Ca) as well as first-row transition metals (M = Sc, V, Fe, Co, Ni) also showed similar structures including enhanced reactivities.[7–10] Moreover, boron clusters and alloys have been proposed for various potential applications, such as building blocks for supramolecular assemblies, hydrogen storage, hydrophilic substances, and protective coatings against corrosion, among others.[10–13]

Recently, Yue *et al.* investigated the fluxional and dynamic behavior of the Al_2B_8 cluster, which was determined by two isolated Al atoms situated above and below the B_8 wheel.[14] Subsequently, Rodríguez–Kessler studied the Al_2B_7 cluster and identified the classical inverse sandwich structure, which contrasts with the Al_2-supported B_8 wheel structure pattern observed in Al_2B_8.[15] In addition, Merino *et al.* discussed the exploration of $TM_2B_7^-$ and TM_2B_8 (TM = Zn, Cd, Hg), denoting a boron centered wheel, involving a fluxional behavior of the TM_2 motif ascribed as molecular stirrers.[16] In order to complete the series of TM_2 doped B_7 cluster, in this work, we have calculated the structure and stability of the Zn_2B_7 cluster. The results show that B_7Zn_2 is formed by two metals lying above a boron centered B_7 wheel, depicting a similar structure to related anionic clusters.[16] In particular, the Zn–Zn distance is in striking contrast to the 4.680 Å in the isolated neutral dimer,[17,18] where the formation of highly elusive Zn–Zn bonds

[a] Centro de Investigaciones en Óptica A.C.,
Loma del Bosque 115, Lomas del Campestre, Leon, 37150, Guanajuato, Mexico.
E-mail: plkessler@cio.mx

[b] Facultad de Ingeniería, Arquitectura y Diseño, Universidad San Sebastián,
Department and Organization, Bellavista 7, 8420524, Santiago, Chile.
E-mail: alvaro.munozc@uss.cl

This journal is © the Owner Societies 2025

Phys. Chem. Chem. Phys., 2025, **27**, 3583–3587 | **3583**

has been realized only after the report by Resa *et al.* in 2004,[19] triggering efforts to understand and increase the libraries of species featuring Zn–Zn direct bonds.[18,20] In this report, we set out to explore the structural, vibrational, and electronic properties of neutral B_7Zn_2, providing insights into the requirements to induce the formation of a direct Zn–Zn bond and the role of the B_7 wheel acting as a ligand. Besides, we evaluated the global minimum and related high-lying isomers by using a modified basin-hopping (MBH) structure search approach, where the bonding characteristics were estimated *via* energy decomposition analysis (EDA), leading to the characterization of the Zn–Zn bonding scheme. Our results provide a beneficial background encouraging further design of plausible species leading to the formation of Zn–Zn bonds.

2. Computational details

Calculations performed in this work are carried out by using density functional theory (DFT) as implemented in the Orca quantum chemistry package.[21] The exchange and correlation energies are addressed by the PBE0 functional in conjunction with the Def2TZVP basis set.[22,23] Atomic positions are self-consistently relaxed through a quasi-Newton method employing the BFGS algorithm. The SCF convergence criteria for geometry optimization are achieved when the total energy difference is smaller than 10^{-8} a.u., by using the TightSCF keyword in the input. The van der Waals interactions are included in the exchange–correlation functionals with empirical dispersion corrections of Grimme DFT-D3(BJ). The total density of states (DOS) and partial density of states (PDOS) for clusters and complexes were obtained by using the Multiwfn program.[24] The IR spectra are obtained by standard diagonalization of the Hessian matrix by using the NumFreq keyword in the input.

3. Results

The structures of the B_7Zn_2 clusters are obtained using a modified basin-hopping (MBH) structure search method over
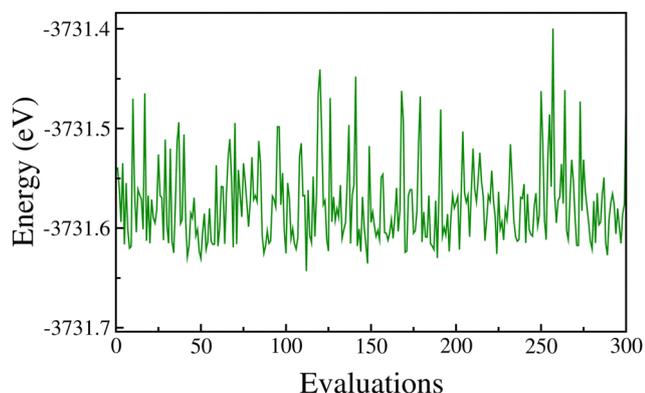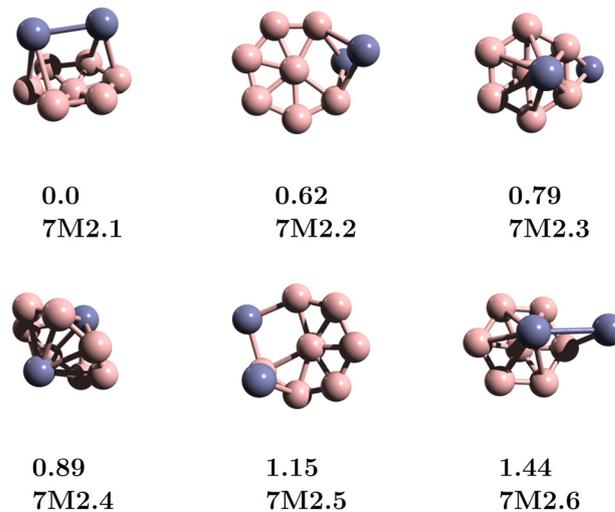

Fig. 2 Lowest energy structures for the B_7Zn_2 clusters. For simplicity, the isomers are denoted by 7M2.*y* (*y* = 1–6).[15] For each structure, the relative energy (in eV) and isomer label are given.

seven generations, as illustrated in Fig. 1. The MBH modified basin-hopping method (MBH) includes random exchanges of atomic species along with standard random perturbations to explore efficiently all possible combinations in the binary alloy.[15,25] The results show that the lowest energy structure for the B_7Zn_2 cluster is a Zn_2-bicapped B_7 wheel 7M2.1. This is in contrast to previous reports on B_7M_2 clusters with early transition metals (M = Sc, Ti, V, Cr), which found inverse sandwich structures like the 7M2.4 isomer, to represent the most stable structure. For 7M2.2, we found a peripheral Zn_2-doped B_7 structure with a relative energy of 0.62 eV (Fig. 2), while the 7M2.3 and 7M2.4 isomers have relative energies of 0.79 and 0.89 eV, respectively.

According to the structures found, we explore the thermodynamic stability of the clusters by using molecular dynamics MD simulations as implemented in the Orca code. The default velocity Verlet algorithm in the NVT ensemble at the PBE/def2-SVP level of theory is set. A timestep of 0.5 femtoseconds and initial velocities according to a temperature of 300 K are used. Temperature is maintained at 300 K using a Berendesen thermostat.[26] The simulations are performed for a time of 1 ps with 0.5 fs of time step. The behavior of the mean square displacement ⟨msd⟩ as a function of time allows us to determine the average bond-length variations during MD simulation, which is evaluated as

$$\langle \text{msd} \rangle = \frac{1}{N} \sum_{i=1}^{N} \left[r_i(t) - r_i(0) \right]^2 \quad (1)$$

where $r_i(t)$ is the position vector in the i-th atom at the time t and N is the total number of atoms in the system. The ⟨msd⟩ parameter allows us to rationalize the dynamical behavior of the clusters.[27,28] In a rigid system, the ⟨msd⟩ parameter remains constant, where in a non-rigid system the ⟨msd⟩ shows variations as a function of time. Upon evaluating the 7M2.1 and

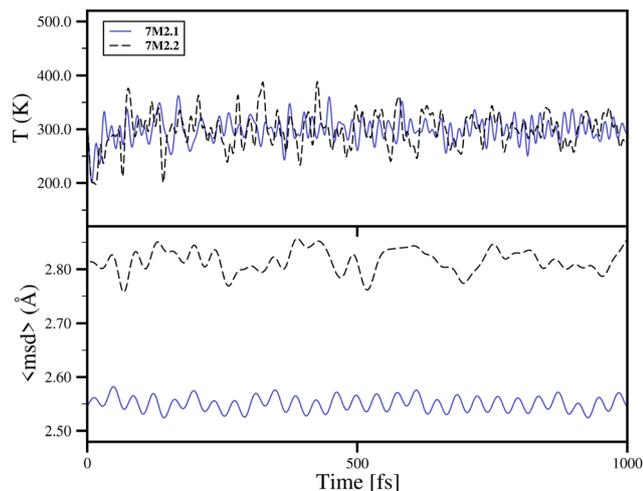Fig. 1 Potential energy surface obtained by a modified basin hopping (MBH) for B_7Zn_2 clusters.

Fig. 3 Temperature (T) and mean square displacement $\langle msd \rangle$ during molecular dynamics simulation for 7M2.1 and 7M2.2 clusters at 300 K.

7M2.2 structures, we found that the clusters exhibit fluxional behavior, which is more pronounced in 7M2.1 (Fig. 3).

To further characterize the B_7Zn_2 clusters, we have calculated the infrared (IR) spectrum, which serves as a guide for future experimental studies.[29,30] For the most stable configurations 7M2.1 and 7M2.2, we found dispersed peaks in the regions of 57.92–1141.60 cm^{-1} and 78.81–1428.16 cm^{-1}, respectively, as shown in Fig. 4. However, 7M2.2 presents a more symmetrical spectrum with a main peak in 826.25 cm^{-1}, while in 7M2.1, the main peak is situated at 1127.62 cm^{-1}. The high-intensity peaks correspond to the stretching vibrations of the central B atom toward the B_7 wheel, whereas other vibrational modes represent distortions of the B atoms, as depicted in Table S4 (ESI†).

To get insight into the electronic properties of the clusters, the total density of states (TDOS) for the 7M2.1 and 7M2.2 clusters is depicted in Fig. S2 (ESI†). For 7M2.1, the PDOS shows more dispersed states, while for 7M2.2 it shows more localization near the HOMO state. The HOMO–LUMO gap for the 7M2.1 and 7M2.2 clusters amounts to 3.43, and 3.75 eV, respectively. The inverse sandwich structure exhibits a smaller gap of 2.07 eV (see Table S3, ESI†). Additionally, the ionization energy of the clusters ranges from 7.40 to 8.27 eV, indicating
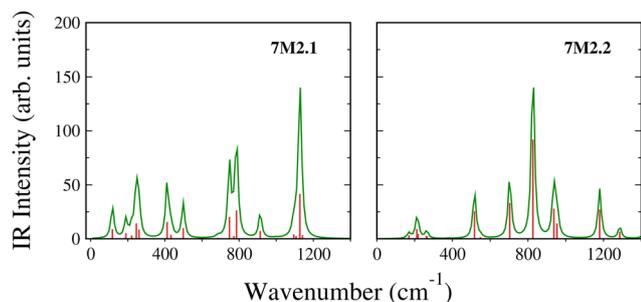

Fig. 4 IR spectra for 7M2.1 and 7M2.2 clusters obtained at the PBE0/Def2-TZVP level.

Table 1 Energy decomposition analysis of the relative energy ($\Delta E_{relEner}$) between B_7Zn_2 isomers. Values in eV

	Rel. ene.	$\Delta E_{Pauli}^{relEner}$	$\Delta E_{Elsta}^{relEner}$	$\Delta E_{Orb}^{relEner}$	$\Delta E_{Disp}^{relEner}$	$\Delta E_{electronic}$	ΔE_{steric}
7M2.1	0.00	0.00	0.00	0.00	0.00	0.00	0.00
7M2.2	0.62	−16.05	5.91	10.73	0.03	16.67	−16.05
7M2.3	0.79	1.62	−0.81	−0.04	0.02	−0.83	1.62
7M2.4	0.89	−6.62	−0.16	7.67	−0.01	7.51	−6.62
7M2.5	1.15	−19.24	7.19	13.18	0.02	20.39	−19.24
7M2.6	1.44	−1.72	0.28	2.87	0.01	3.16	−1.72

their exceptional electronic stability. Based on this analysis, the most stable clusters are less reactive compared to the higher-energy isomers.

In order to evaluate the factors governing the stabilization of the global minimum (7M2.1) in relation to high-lying isomers, energy decomposition analysis (EDA) was performed as implemented in the ADF2024 code,[31] where the relative energy is dissected in different meaningful terms given by the repulsive Pauli ($\Delta E_{Pauli}^{relEner}$), orbital interaction ($\Delta E_{Orb}^{relEner}$), electrostatic contribution ($\Delta E_{Elsta}^{relEner}$), and dispersion term ($\Delta E_{Disp}^{relEner}$),[32] which accounts for electronic ($\Delta E_{Elsta}^{relEner} + \Delta E_{Orb}^{relEner} + \Delta E_{Disp}^{relEner}$) and steric ($\Delta E_{Pauli}^{relEner}$) contributions (Table 1). The obtained results exhibit several differences between isomers where despite the lesser steric repulsion provided in 7M2.2, a destabilization of the electronic terms, mainly given by the electrostatic character, ensures 7M2.1 as the global minimum. For 7M2.3, the stabilizing electronic contribution is similar to 7M2.1; however, introducing a slightly larger destabilizing steric repulsion. For 7M2.4, 7M2.5, and 7M2.6, the situation is similar to 7M2.2, thus denoting that the decrease in electronic stabilizing contribution is the main factor in determining the global minimum.

For the inverse sandwich isomer, the atomic radii of Zn (1.22 Å)[33] are larger to be placed above the B_7 ring, which involves an available radius of 1.0 Å ($B_7^{diameter}$ − B^{radii} = 1.809 − 0.84 Å = 0.969 Å), which leads to a destabilization of the structure by steric factors (Table 1). In addition, the evaluation of the aromatic properties of 7M2.4 unravels an antiaromatic character (Fig. 5), in line with the electronic destabilization mostly given by the decrease in orbital interactions (Table 1), which are key features to enable electronic delocalization in the overall structure. In this framework, an induced central shielding region is indicative of an aromatic behavior, whereas a central deshielding region accounts for an antiaromatic behavior.[34,35] For 7M2.4, a central deshielding region is found, which is indicative of an antiaromatic behavior, also noted for both bare B_7 structures. In contrast, 7M2.1 exhibits a decrease in the parent antiaromatic behavior of B_7, leading to more aromatic characteristics, as noted by the shielding region at the center of the structure (blue color).

The EDA analysis of the Zn_2–B_7 interaction denotes an energy of −2.78 eV, which is mostly provided by the stabilizing contribution of the orbital interaction (55.0%, Table S1, ESI†), and from the electrostatic character (43.8%), which involves a sizable $Zn_2 \rightarrow B_7$ net charge transfer of 0.60 e, involving a

This journal is © the Owner Societies 2025
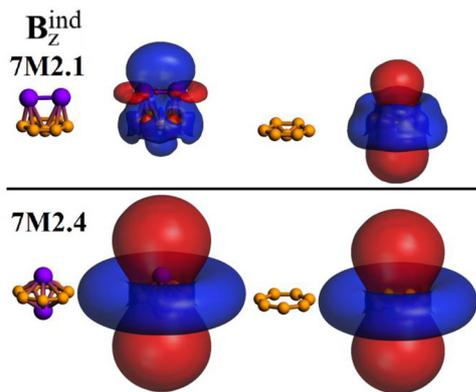
Phys. Chem. Chem. Phys., 2025, **27**, 3583–3587 | **3585**

Fig. 5 Induced magnetic field under a perpendicular field (B_z^{ind}), showing an antiaromatic character for both bare B_7 structures, and the inverse sandwich 7M2.4, given the formation of a deshielding region at the center of the structure. Color code: blue: shielding/red: deshielding. Isosurface values set at $\pm$ 3.0 ppm.

bonding between Zn_2 and π-orbitals of B_7 (Fig. S1, ESI†). Interestingly, the charge transfer in turn leads to a reorganization of the population of σ-Zn_2 orbitals (Table S2, ESI†), resulting in 1.94 e in σ, 0.81 e in σ^*, and population of the initially unoccupied π-Zn_2 of 0.61 e. Such a charge reorganization in the B_7 supported Zn_2 dimer increases the bonding contribution (π-Zn_2) and decreases the antibonding character (σ^*-Zn_2), resulting in a Mayer bond order[36,37] of 0.50, denoting the formation of a formal Zn–Zn bond weaker that a single bond. For the related anionic counterpart, $Zn_2B_7^-$, the Zn_2–B_7 interaction energy amounts to -2.88 eV, with a $Zn_2 \rightarrow B_7$ net charge transfer of 0.33 e, where the incoming electrons reside mainly at the B_7 motif. The population of Zn_2 based orbitals in the anionic species is of σ-Zn_2 1.92 e, σ^*-Zn_2 0.92 e, π-Zn_2 0.79 e, denoting a similar situation to the neutral counterpart, with a calculated Zn–Zn Mayer bond order of 0.33. Based on the net bonding electrons of σ- and π-Zn_2 orbitals, the resulting Zn–Zn bond order is given by 64.8% from σ- and 35.2% from π-character in the neutral Zn_2B_7, and of 55.9% and 44.1% respectively, for the anionic counterpart. Thus, the role of B_7 as an electron-acceptor motif acting as a ligand for the Zn_2 dimer ensures the depopulation of the antibonding character, and increases the population of bonding orbitals, leading to the formation of an intermediate Zn–Zn bond, in both neutral and anionic counterparts. Hence, the introduction of more electron-deficient supporting ligands may be able to increase the Zn–Zn bond order, encouraging the quest for the formation of single or larger Zn–Zn bond orders.

4 Conclusions

In this work, we employed density functional theory (DFT) to explore the structure of boron clusters doped with two zinc atoms (B_7Zn_2 or Zn_2B_7). The results showed that the most stable structure is a B_7-supported Zn_2 dimer, which is 0.89 eV lower in energy compared to the classical inverse-sandwich structure adopted in B_7TM_2 (TM = transition metal) clusters.

The characteristics of these systems are evaluated by the IR spectra, density of states, and bonding analyses. The formation of the Zn–Zn intermediate bond order is given by the electron-acceptor characteristics of the B_7 motif, leading to a depopulation of antibonding Zn–Zn orbitals, and, population of the respective bonding orbitals, highlighting the role of both σ- and π-Zn_2 orbitals, in the resulting bond order. Interestingly, in the light of such findings, the quest for the design and feasible characterization of Zn–Zn bonded structures may be triggered by the use of more electron-deficient supporting ligands, as a key factor towards obtaining larger Zn–Zn elusive bond orders in stable species.

Data availability

The data supporting the conclusions reached in this study have been included as part of the ESI.†

Conflicts of interest

There are no conflicts to declare.

Acknowledgements

References

1 E. Oger, N. Crawford, R. Kelting, P. Weis, M. Kappes and R. Ahlrichs, Boron Cluster Cations: Transition from Planar to Cylindrical Structures, *Angew. Chem., Int. Ed.*, 2007, **46**, 8503–8506.

2 B. Albert and H. Hillebrecht, Boron: Elementary Challenge for Experimenters and Theoreticians, *Angew. Chem., Int. Ed.*, 2009, **48**, 8640–8668.

3 W.-J. Chen, A. S. Pozdeev, H. W. Choi, A. I. Boldyrev, D.-F. Yuan, I. A. Popov and L.-S. Wang, Searching for stable copper borozene complexes in CuB_7^- and CuB_8^-, *Phys. Chem. Chem. Phys.*, 2024, **26**, 12928–12938.

4 P.-F. Han, Q. Sun and H.-J. Zhai, Boron-Based Inverse Sandwich $V_2B_7^-$ Cluster: Double π/σ Aromaticity, Metal-Metal Bonding, and Chemical Analogy to Planar Hypercoordinate Molecular Wheels, *Molecules*, 2023, **28**(12), 4721.

5 W.-L. Li, L. Xie, T. Jian, C. Romanescu, X. Huang and L.-S. Wang, Hexagonal Bipyramidal $[Ta2B6]^{-/0}$ Clusters: B6 Rings as Structural Motifs, *Angew. Chem., Int. Ed.*, 2014, **53**, 1288–1292.

6 W.-L. Li, T.-T. Chen, D.-H. Xing, X. Chen, J. Li and L.-S. Wang, Observation of highly stable and symmetric lanthanide octa-boron inverse sandwich complexes, *Proc. Natl. Acad. Sci. U. S. A.*, 2018, **115**, E6972–E6977.

3586 | *Phys. Chem. Chem. Phys.*, 2025, **27**, 3583–3587

This journal is © the Owner Societies 2025

7 J. Jia, X. Li, Y. Li, L. Ma and H.-S. Wu, Density functional theory investigation on the structure and stability of Sc_2B_n (n = 1–10) clusters, *Comput. Theor. Chem.*, 2014, **1027**, 128–134.

8 H. T. Pham, M. P. Pham-Ho and M. T. Nguyen, Impressive capacity of the B_7^- and V_2B_7 clusters for CO_2 capture, *Chem. Phys. Lett.*, 2019, **728**, 186–194.

9 H.-R. Li, C. Zhang, W.-B. Ren, Y.-J. Wang and T. Han, Geometric structures and hydrogen storage properties of M_2B_7 (M = Be, Mg, Ca) clusters, *Int. J. Hydrogen Energy*, 2023, **48**, 25821–25829.

10 D. Olalde-López, P. Rodríguez-Kessler, S. Rodríguez-Carrera and A. Muñoz-Castro, Hydrogen storage properties for bimetallic doped boron clusters M_2B_7 (M = Fe, Co, Ni), *Int. J. Hydrogen Energy*, 2024, DOI: **10.1016/j.ijhydene.2024.05.429**.

11 A. Barba-Bon, G. Salluce, I. Lostalé-Seijo, K. I. Assaf, A. Hennig, J. Montenegro and W. M. Nau, Boron clusters as broadband membrane carriers, *Nature*, 2022, **603**, 637–642.

12 P. Álvarez Zapatero, A. Lebon, R. H. Aguilera del Toro, A. Aguado and A. Vega, Why are Zn-rich Zn-Mg nanoalloys optimal protective coatings against corrosion? A first-principles study of the initial stages of the oxidation process, *Phys. Chem. Chem. Phys.*, 2021, **23**, 24685–24698.

13 J. Cebula, K. Fink, J. Boratyński and T. M. Goszczyński, Supramolecular chemistry of anionic boron clusters and its applications in biology, *Coord. Chem. Rev.*, 2023, **477**, 214940.

14 R.-X. Yue, S.-J. Gao, P.-F. Han and H.-J. Zhai, Chemical bonding and dynamic structural fluxionality of a boron-based Al_2B_8 binary cluster: the robustness of a doubly $6\pi/6\sigma$ aromatic $[B_8]^{2-}$ molecular wheel, *RSC Adv.*, 2023, **13**, 1964–1973.

15 P. L. Rodríguez-Kessler, Vibrational and electronic properties of the B_7Al_2 cluster *arXiv*, 2024, preprint, DOI: **10.48550/arXiv.2409.18165**.

16 R. Yu, J. Barroso, M.-H. Wang, W.-Y. Liang, C. Chen, X. Zarate, M. Orozco-Ic, Z.-H. Cui and G. Merino, Structure and bonding of molecular stirrers with formula B7M2 and B8M2 (M = Zn, Cd, Hg), *Phys. Chem. Chem. Phys.*, 2020, **22**, 12312–12320.

17 J. Hicks, E. J. Underhill, C. E. Kefalidis, L. Maron and C. Jones, A Mixed-Valence Tri-Zinc Complex, [LZnZnZnL] (L = Bulky Amide), Bearing a Linear Chain of Two-Coordinate Zinc Atoms, *Angew. Chem., Int. Ed.*, 2015, **54**, 10000–10004.

18 X. Liu, M. Zhang, S. Wu, R. Zhong, Y. Liu, A. M. Arif, Y. Geng and Z. Su, All-Metallic Zn=Zn Double-Bonded Octahedral Zn_2M_4 (M = Li, Na) Clusters with Negative Oxidation State of Zinc, *ChemPhysChem*, 2020, **21**, 459–463.

19 I. Resa, E. Carmona, E. Gutierrez-Puebla and A. Monge, Decamethyldizincocene, a Stable Compound of Zn(I) with a Zn–Zn Bond, *Science*, 2004, **305**, 1136–1138.

20 K. Mayer, L.-A. Jantke, S. Schulz and T. F. Fässler, Retention of the Zn–Zn bond in $[Ge_9Zn–ZnGe_9]_6$ and Formation of $[(Ge_9Zn)(Ge_9)(ZnGe_9)]_8$ and Polymeric $[(Ge_9Zn)_2]$, *Angew. Chem., Int. Ed.*, 2017, **56**, 2350–2355.

21 F. Neese, F. Wennmohs, U. Becker and C. Riplinger, The ORCA quantum chemistry program package, *J. Chem. Phys.*, 2020, **152**, 224108.

22 C. Adamo and V. Barone, Toward reliable density functional methods without adjustable parameters: The PBE0 model, *J. Chem. Phys.*, 1999, **110**, 6158–6170.

23 F. Weigend and R. Ahlrichs, Balanced basis sets of split valence, triple zeta valence and quadruple zeta valence quality for H to Rn: Design and assessment of accuracy, *Phys. Chem. Chem. Phys.*, 2005, **7**, 3297–3305.

24 T. Lu and F. Chen, Multiwfn: A multifunctional wavefunction analyzer, *J. Comput. Chem.*, 2012, **33**, 580–592.

25 P. L. Rodríguez-Kessler, A. R. Rodríguez-Domínguez and A. Muñoz-Castro, Systematic cluster growth: a structure search method for transition metal clusters, *Phys. Chem. Chem. Phys.*, 2021, **23**, 4935–4943.

26 H. J. C. Berendsen, J. P. M. Postma, W. F. van Gunsteren, A. DiNola and J. R. Haak, Molecular dynamics with coupling to an external bath, *J. Chem. Phys.*, 1984, **81**, 3684–3690.

27 G. Martínez-Guajardo, J. Luis Cabellos, A. Díaz-Celaya, S. Pan, R. Islas, P. K. Chattaraj, T. Heine and G. Merino, Dynamical behavior of Borospherene: A Nanobubble, *Sci. Rep.*, 2015, **5**, 11287.

28 R. A. Murcia-Galán, S. M. Durán, S. M. Leal-Pinto, M. V. Roa-Cordero, J. D. Vargas, L. V. Herrera, A. Muñoz-Castro, D. MacLeod-Carey, T. W. Naranjo, P. L. Rodríguez-Kessler and J. J. Hurtado, Antifungal activity of Co(II) and Cu(II) complexes containing 1,3-bis(benzotriazol-1-yl)-propan-2-ol on the growth and virulence traits of fluconazole-resistant Candida species: synthesis, DFT calculations, and biological activity, *BMC Chem.*, 2023, **17**, 135.

29 L. Wen, G. Li, L.-M. Yang and E. Ganz, Structural evolution in boron-based clusters $B_5Aln^{0/-/+}$ (n = 1–4): Al atoms transition from the periphery of the planar W-shaped B_5 ring to the vertex of the bipyramid, *Eur. Phys. J. D*, 2020, **74**, 223.

30 P. L. Rodríguez-Kessler, Revisiting the Global Minimum Structure of the Pt_5 V Cluster *arXiv*, 2024, preprint, DOI: **10.48550/arXiv.2408.03537**.

31 *ADF 2024.1, SCM*, Theoretical Chemistry, Vrije Universiteit, Amsterdam, The Netherlands, 2024, **https://www.scm.com**.

32 S. Ehrlich, J. Moellmann and S. Grimme, Dispersion-Corrected Density Functional Theory for Aromatic Interactions in Complex Systems, *Acc. Chem. Res.*, 2013, **46**, 916–926.

33 B. Cordero, V. Gómez, A. E. Platero-Prats, M. Revés, J. Echeverría, E. Cremades, F. Barragán and S. Alvarez, Covalent radii revisited, *Dalton Trans.*, 2008, 2832–2838.

34 G. Merino, T. Heine and G. Seifert, The Induced Magnetic Field in Cyclic Molecules, *Chem. – Eur. J.*, 2004, **10**, 4367–4371.

35 R. Islas, T. Heine and G. Merino, The Induced Magnetic Field, *Acc. Chem. Res.*, 2012, **45**, 215–228.

36 A. J. Bridgeman, G. Cavigliasso, L. R. Ireland and J. Rothery, The Mayer bond order as a tool in inorganic chemistry, *J. Chem. Soc., Dalton Trans.*, 2001, 2095–2108.

37 I. Mayer, Bond order and valence indices: A personal account, *J. Comput. Chem.*, 2007, **28**, 204–221.

This journal is © the Owner Societies 2025

Phys. Chem. Chem. Phys., 2025, **27**, 3583–3587 | **3587**